Nanoscale

Accepted Manuscript

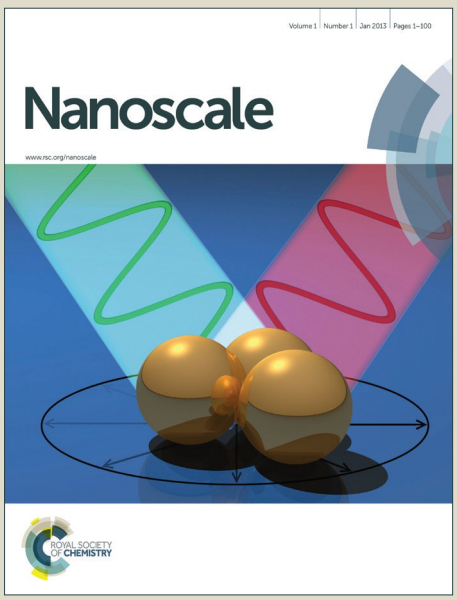

ROYAL SOCIETY OF CHEMISTRY

www.rsc.org/nanoscale

Journal Name

RSCPublishing

COMMUNICATION

In situ clicking methylglyoxal for hierarchical self-assembly of nanotubes in supramolecular hydrogel

Cite this: DOI: 10.1039/x0xx00000x

Shuang Liu, Yufeng Luo and Gaolin Liang*

Received 00th January 2012,
Accepted 00th January 2012

DOI: 10.1039/x0xx00000x

www.rsc.org/

Methylglyoxal (MGO) is a toxic, dicarbonyl metabolite in all living cells and its detoxification is regulated by glyoxalase I (GLOI). Herein, we rationally designed a precursor *o*-phenylenediamine-Phe-Phe-OH (1) which "click" reacts with MGO to yield amphiphilic methylquinoxaline-Phe-Phe-OH (2) to self-assemble into supramolecular hydrogel II (Gel II). Cryo-TEM images of Gel II suggested that there existed two orders of self-assembly to form the 32.8 nm-width-nanotubes in the hydrogel. The hypothesis was validated with the analyses of the fluorescence, transmittance, and circular dichroism data of the serial dilutions of Gel II. Interference tests indicated that hydrogelation of 1 with MGO would not be affected by nitric oxide (NO). Our results suggest that 1 could be applied for specific hydrogelation with MGO, and potentially the removal of MGO *in vitro*.

Methyglyoxal (MGO), a small molecular reactive dicarbonyl, exists in all living cells during their glucose, amino acid, and fatty acid metabolism.[1] It can directly glycate both proteins and DNA to yield the advanced glycation end-products (AGEs), causing activation of membrane receptors, dysfunction of the proteins, or induction of pro-inflammatory signaling which respectively link to diabetic complications, aging disorders, or chronic inflammation.[2] Among the MGO-associating diseases, connection of diabetes with MGO is particularly notable because levels of MGO in the plasma of diabetics have been found consistently increased.[3] In cellular systems, MGO has also been found to impose a number of deleterious effects on the cells including inflammation, oxidative stress, defects in cell adhesion, and even dysfunction.[4] In cells, glyoxalase I (GLOI) catalyzes the formation of S-D-lactoylglutathione from MGO and glutathione (GSH), thus regulating the detoxification of MGO.[5] Spiegel and co-workers developed an *o*-phenylenediamine (OPD)-based fluorophore precursor to quickly trap MGO and thereafter turn on the fluorescence for specific detection of MGO.[6]

Supramolecular hydrogels, due to their inherent biocompatibility and degradability, have been extensively explored and found wide applications in wound healing,[8] drug delivery,[9-12] and tissue engineering.[13] In 2006, Xu and co-workers used sol-gel-sol transitions to observe the activity of alkaline phosphatase and kinase with naked eyes.[14] Liang and co-workers invented a bipyridine-based supramolecular hydrogel for not only sensing Cd^{2+} with high sensitivity and selectivity, but also visible Cd^{2+} removal.[15]

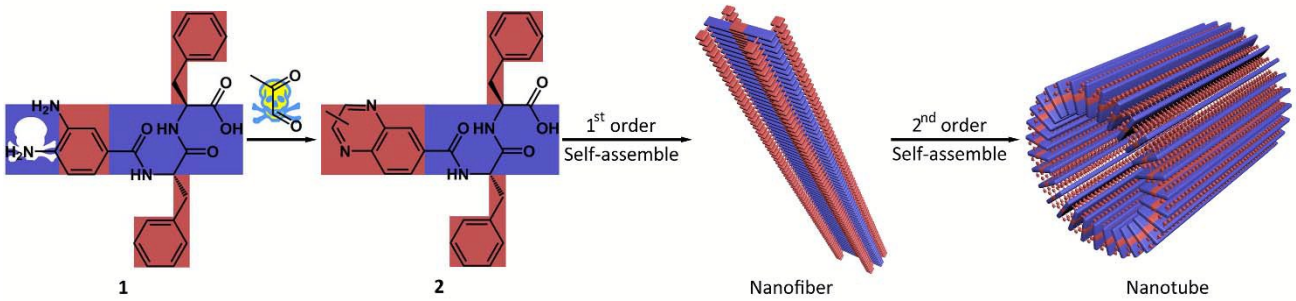

Scheme 1 Schematic illustration of using precursor **1** to in situ click methylglyoxal for hierarchical self-assembly of nanotubes in supramolecular hydrogel. Blue parts indicate hydrophilic structures, red parts indicate hydrophobic structures.

Journal Name RSCPublishing

COMMUNICATION

Click reaction, a highly- selective and yielding chemical approach,[16-20] has been utilized in hydrogelation, but mostly for crosslinking of the gelators.[21, 22] There are very few works of using click reactions to in situ synthesize the gelators for the preparation of the hydrogels.[23, 24] Inspired by above pioneering works and considering the high efficiency of click reaction, we devoted to design a hydrogelator precursor which can in situ "click" react with MGO to form supramolecular hydrogel. This in situ hydrogelation process can be potentially applied for detoxification and removal of MGO *in vitro*. Thus, as shown in Scheme 1, we rationally designed a precursor *o*-phenylenediamine-Phe-Phe-OH (OPD-FF, **1**) for this purpose with following components: (1) a typical FF motif for self-assembly of fibrous structures in supramolecular hydrogel;[25, 26] (2) an OPD motif for clicking MGO to yield the hydrogelator methylquinoxaline-Phe-Phe-OH (MQ-FF, **2**) whose aromatic MQ motif provides π-π interactions for molecular self-assembly. Unlike a typical "annealing" hydrogelation process which changes the interaction force between the hydrogelator and water by changing temperature,[27-29] this hydrogelation process involves a direct change of the hydrophilicity of the precursor by in situ click reaction to yield the amphiphilic hydrogelator. Surprisingly, we found that there existed two orders of self-assembly in this hydrogel. The 1st order of self-assembly was that of **2** to form nanofibers with average diameter of 3.1 nm. The 2nd order of self-assembly was coiling of afore nanofibers to form bigger nanotubes with average outer diameter of 32.8 nm.

We began the study with the syntheses of precursor **1** (Scheme S1, Electronic Supplementary Information). In detail, overnight reaction between 3,4-diaminobenzoic acid and 9-fluorenylmethyloxycarbonyl chloride in 10% $NaHCO_3$ solution yielded $(Fmoc)_2$-OPD-OH (**A**) with good yield. $(Fmoc)_2$-OPD-FF-OH (**B**) was then synthesized with solid phase peptide synthesis (SPPS) using Fmoc-Phe-OH and **A**. Deprotection of **B** with 10% piperidine in dimethylformamide (DMF) yielded precursor **1** after HPLC purification.

After obtaining **1**, we tested its feasibility of hydrogelation. Dissolving 2.2 mg **1** in 200 μL phosphate buffer (0.2 M, pH 7.4) in a vial resulted in a clear solution of **1** at 25.0 mM. After applying the solution with a heat up-cool down process, we observed that it was still a clear solution (left vial in Fig. 1A), suggesting that precursor **1** itself could not form a hydrogel at this concentration. After addition of equivalent MGO to the solution and the reaction mixture was left to stand at room temperature for one hour, a little bit turbid supramolecular hydrogel II (Gel II) formed in the vial (right vial in Fig. 1A). Inverted tube test indicated that the critical gelation concentration (CGC) for Gel II is 20.5 ± 0.5 mM (Fig. S6). To evaluate the viscoelastic properties of Gel II at 25.0 mM, we firstly used dynamic strain sweep to determine the proper condition for the dynamic frequency sweep of the hydrogel. As shown in Fig. S7 in Electronic Supplementary Information, the values of the storage modulus (G') and the loss modulus (G") of Gel II exhibit a weak dependence from 0.01% to 1.0% of strain (with G' dominating G"), indicating that the sample is hydrogel. After setting the strain amplitude at 0.50% (within the linear response regime of strain amplitude), we used dynamic frequency sweep to study Gel II. As shown in Fig. 1B, the G' and G" of Gel II slightly increase with the increase of frequency from 0.01 to 10 Hz. The values of G' are about 5 times larger than those of G" in this range (0.01 to 10 Hz), suggesting that Gel II is fairly tolerant to external shear force.

To chemically characterize the composition of the hydrogel, we directly dissolved Gel II in 10% CH_3CN in water and injected the mixture into a high-performance liquid chromatography (HPLC) system for analysis. As shown in Fig. S8 in Electronic Supplementary Information, HPLC peak of precursor **1** at retention time of 19.1 min almost disappeared from the trace of Gel II while a new peak at retention time of 24.1 min appeared.

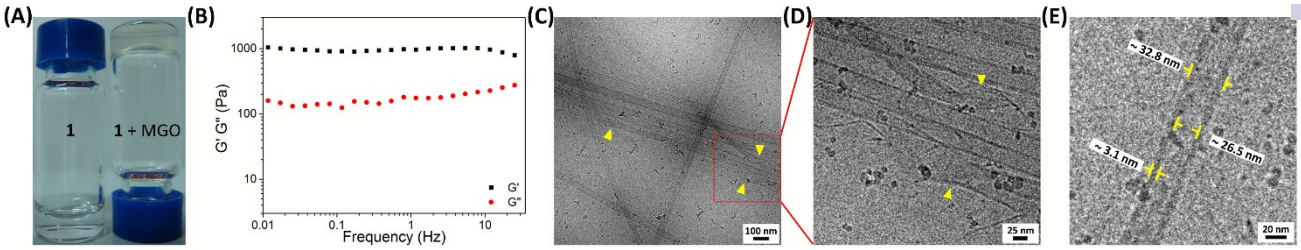

Fig. 1 (A) Photographs of solution of **1** at 25.0 mM in buffer (left) and hydrogel Gel II in situ formed from click reaction between equivalent **1** and MGO at 25.0 mM (right). (B) Dynamic frequency of storage modulus (G') and the loss modulus (G") of Gel II at the strain of 0.50%. Condition: [**1**] = [MGO] = 25.0 mM, pH 7.4, room temperature. (C) Cryo-TEM image of Gel II. (D) Magnified image of the red square area in C. (E) High magnification of Cryo-TEM image of Gel II to show the nanotubes in detail.

Journal Name RSCPublishing

COMMUNICATION

Collecting the new peak and characterizing it with proton nuclear magnetic resonance (^{1}H NMR), carbon NMR (^{13}C NMR), and high-resolution mass (HRMS) spectra (Figs. S9-11), we did confirm that the new peak was the hydrogelator **2**, suggesting that the click reaction between MGO and the OPD motif of **1** was clean and efficient.

To investigate the fibrous networks in Gel II, we performed cryo transmission electron microscopy (cryo-TEM) observations. At low magnification, the microscopic structure of Gel II under cryo-TEM exhibited long fibers with lengths normally more than ten microns (Fig. S12). Higher magnification of cryo-TEM images of Gel II indicated that afore fibrous structures were nanotubes but not nanobundles (Fig. 1C). At the ends of the nanotubes, we could find that the nanotubes were self-assembled from the parallel alignment of smaller nanofibers (indicated by yellow arrow heads in Fig. 1C and 1D). Cryo-TEM images of the reaction mixtures of **1** and equivalent MGO at lower concentrations (5 mM and 10 mM) indicated the presence of nanofibers for self-assembling into the nanotubes (Fig. S13). Statistical analysis indicated that the nanotubes had an average outer diameter of 32.8 ± 1.5 nm and an average inner diameter of 26.5 ± 2.0 nm (Fig. 1E). And the average width of the nanotube walls was calculated to be 3.1 ± 0.2 nm (Fig. 1E), which was close to that of nanofibers self-assembled from small molecules with similar molecular weight to **2**.[24] This echoed that the nanotubes were self-assembled from the parallel alignment of 3.1 nm-diameter-nanofibers of **2**, as proposed in Scheme 1.

Based on the cryo-TEM observations, we hypothesized that there existed two orders of self-assembly in Gel II. The 1st order of self-assembly was responsible for the formation of 3.1 nm-diameter-nanofibers while the 2nd order of self-assembly was responsible for the formation of 32.8 nm-width-nanotubes. To testify this hypothesis, we dispersed Gel II in afore phosphate buffer and obtained serial dilutions at concentrations ranging from 2.44 μM to 5.00 mM. Participation of the MQ moiety of **2** in the gelation, which was responsible for the 1st order of self-assembly of the nanofibers, was investigated by measuring the fluorescence spectra of the serial dilutions excited at 280 nm. The results indicated that the fluorescence emission maximums of the dilutions red shifted from 340 nm to 365 nm with the increases of their concentrations (Fig. S14A). The significant red shifts of the fluorescence indicate the π-π interactions among the MQ motifs of the hydrogelator **2**. Plots of fluorescence emission maximum versus logarithm of concentration revealed two regimes, indicating the critical micelle concentration (CMC) for the 1st order self-assembly of nanofibers is 21.8 μM (Fig. 2A). Since the 2nd order self-assembly in Gel II (i.e., parallel alignment of nanofibers to form nanotubes) resulted from the π-π interaction among the phenyl groups of the Phe motifs on **2**, which would not impact additional change of the fluorescence of the MQ motifs on **2**, indeed have not we found the third regime in Fig. 2A. Nevertheless, the 2nd order self-assembly of nanotubes in bigger sizes should result in transmittance change of the dilutions (suggested by the turbidity of Gel II in Fig. 1A). Therefore, we measured the transmittances of these dilutions (Fig. S14B), plotted their transmittances at 425 nm versus their concentrations and showed the results in Fig. 2B. The plots revealed two regimes, indicating a CMC 402 μM for the 2nd order self-assembly of the nanotubes in Gel II. To further validate the hierarchical self-assembly in the nanotubes, we conducted circular dichroism (CD) spectroscopy measurements on the serial dilutions of Gel II. As shown in Fig. 2C, at concentrations higher than 21.8 μM but lower than 402 μM, clearly we observed two troughs at 206 nm (ππ* transition) and 238 nm (nπ* transition), which represent random coil and β-turn structures, respectively.[27, 28] Appearance of these two troughs indicated the 1st order self-assembly o nanofibers in the dilutions. At a concentration of 781 μM, CD spectrum of the dilution exhibited a trough at about 319 nm,

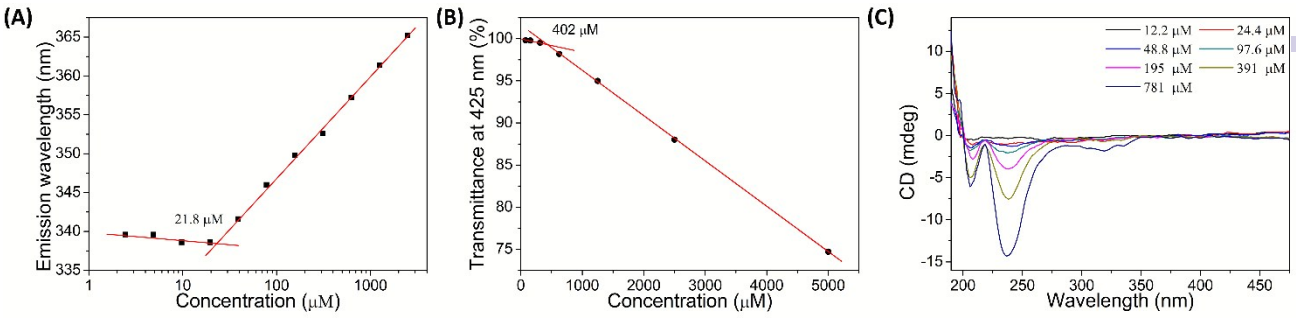

Fig. 2 (A) Gelator concentration-dependent fluorescence emission maximum of dilutions of Gel II. Excitation: 280 nm. (B) Gelator concentration-dependent optical transmittance at 425 nm of dilutions of Gel II. (C) Circular dichroism spectra of dilutions of Gel II.

Journal Name RSCPublishing

COMMUNICATION

indicating the chiral arrangement of the aromatic side chains of **2**,[30] which suggests the 2nd order self-assembly of nanofibers to form the nanotubes. These above results strongly suggested that our precursor **1** could in situ click MGO for hierarchical self-assembly of nanotubes and thereafter form supramolecular hydrogel.

In MGO-OPD click reaction-based systems, nitric oxide (NO), a ubiquitous signalling molecule in various physiological systems, is a usual interference. This is because OPD can also irreversibly react with NO^+ or N_2O_3 to form benzotriazole derivatives.[6, 31] Thus, in this work, we also studied the interference of NO with MGO-**1** hydrogelation. To the 25.0 mM solution of **1** in phosphate buffer, 5 equiv. of NO was injected in half an hour. After a heat up-cool down process, the reaction mixture was left to stand at room temperature for another hour, resulting in a dark red solution III (Sol III) (Fig. S15). HPLC analysis indicated that the precursor **1** was almost converted into a new compound with retention time of 21.6 min (Fig. S16). Characterizations of the new compound with ^{1}H NMR and HRMS spectra (Figs. S17 and S18) confirmed it to be expected benzotriazole-Phe-Phe-OH (**3**, Scheme S2). Cryo-TEM image of Sol III showed that there was neither nanofiber nor nanotube in it (Fig. S19). To test the interference of NO with the hydrogelation process of **1** and MGO, we simultaneously added equivalent MGO and NO to the 25.0 mM solution of **1** and the reaction mixture was left to stand at room temperature for one hour. Clearly we found a brown supramolecular hydrogel formed in the vial (Fig. S20A). Quantitative HPLC analysis indicated that the precursor **1** was converted to **2** in the majority and **3** in the minority at a molar ratio of 7.8 : 1 (Fig. S20B-D). These above results indicate that our precursor **1** can be used to click MGO for specific hydrogelation with MGO without interference from NO.

Conclusions

In summary, we rationally designed a precursor **1** which can click react with MGO to yield amphiphilic MQ derivative **2** for hierarchical self-assembly of nanotubes in hydrogel II (Gel II). Inverted tube test indicated that the CGC for MGO to form Gel II was 20.5 mM. Cryo-TEM images of Gel II suggested that there existed two orders of self-assembly to form the nanotubes in the hydrogel. The 1st order of self-assembly of **2** was responsible for the formation of 3.1 nm-diameter-nanofibers while the 2nd order of self-assembly of the nanofibers resulted in the formation of 32.8 nm-width-nanotubes. This hypothesis was validated with the analyses of the fluorescence, transmittance, and CD data of the serial dilutions of Gel II. Interference tests indicated that hydrogelation of **1** with MGO would not be affected by NO. These above results suggest that our compound **1** could be applied for specific hydrogelation with MGO, and potentially the removal of MGO *in vitro*.

Acknowledgements

The authors are grateful to Prof. Zhigang Wang for his assistance in the rheology study. This work was supported by Collaborative Innovation Center of Suzhou Nano Science and Technology, the Major program of Development Foundation of Hefei Center for Physical Science and Technology, and the National Natural Science Foundation of China (Grants U1532144 and 21375121).

Notes and references

CAS Key Laboratory of Soft Matter Chemistry, National Synchrotron Radiation Laboratory, Department of Chemistry, University of Science and Technology of China, 96 Jinzhai Road, Hefei, Anhui 230026, China

E-mail: gliang@ustc.edu.cn (G.-L. L.).

† Electronic Supplementary Information (ESI) available: Additional experimental details as described in text. Synthetic routes for **1**: Schemes S1-S2, Figures S1-S20 and Table S1. See DOI: 10.1039/c000000x/

1 M. P. Kalapos, *Toxicol. Lett.*, 1999, **110**, 145-175.
2 P. Matafome, C. Sena and R. Seiça, *Endocrine*, 2013, **43**, 472-484.
3 M. P. Kalapos, *Diabetes Res. Clin. Pract.*, 2013, **99**, 260-271.
4 L. Y. Wu and B. H. J. Juurlink, *Hypertension*, 2002, **39**, 809-814.
5 S. C. Chauhan and R. Madhubala, *PLoS One*, 2009, **4**, e6805.
6 T. Wang, E. F. Douglass, Jr., K. J. Fitzgerald and D. A. Spiegel, *J. Am. Chem. Soc.*, 2013, **135**, 12429-12433.
7 B. Mei, Q. Q. Miao, A. M. Tang and G. L. Liang, *Nanoscale* 2015, **7**, 15605-15608.
8 Z. M. Yang, G. L. Liang, M. L. Ma, A. S. Abbah, W. W. Lu and B. Xu, *Chem. Commun.*, 2007, 843-845.
9 G. L. Liang, Z. M. Yang, R. J. Zhang, L. H. Li, Y. J. Fan, Y. Kuang, Y. Gao, T. Wang, W. W. Lu and B. Xu, *Langmuir*, 2009, **25**, 8419-8422.
10 Y. Yu and Y. Chau, *Biomacromolecules*, 2015, **16**, 56-65.
11 J. Wei, H. M. Wang, M. F. Zhu, D. Ding, D. X. Li, Z. N. Yin, L. Y. Wang and Z. M. Yang, *Nanoscale*, 2013, **5**, 9902-9907.
12 T. Su, Z. Tang, H. J. He, W. J. Li, X. Wang, C. A. Liao, Y. Sun and Q. G. Wang, *Chem. Sci.*, 2014, **5**, 4204-4209.
13 J. A. Burdick and W. L. Murphy, *Nat. Commun.*, 2012, **3**, 2169.
14 Z. M. Yang, G. L. Liang, L. Wang and B. Xu, *J. Am. Chem. Soc.*, 2006, **128**, 3038-3043.

15 Q. Q. Miao, Z. Y. Wu, Z. J. Hai, C. L. Tao, Q. P. Yuan, Y. D. Gong, Y. F. Guan, J. Jiang and G. L. Liang, *Nanoscale*, 2015, **7**, 2797-2804.
16 H. C. Kolb, M. G. Finn and K. B. Sharpless, *Angew. Chem. Int. Ed.*, 2001, **40**, 2004-2021.
17 Y. Yuan, D. Li, J. Zhang, X. M. Chen, C. Zhang, Z. L. Ding, L. Wang, X. Q. Zhang, J. H. Yuan, Y. M. Li, Y. B. Kang and G. L. Liang, *Chem. Sci.*, 2015, **6**, 6425-6431.
18 Y. Yuan, L. Wang, W. Du, Z. L. Ding, J. Zhang, T. Han, L. N. An, H. F. Zhang and G. L. Liang, *Angew. Chem. Int. Ed.*, 2015, **54**, 9700-9704.
19 G. L. Liang, H. J. Ren and J. H. Rao, *Nat. Chem.*, 2010, **2**, 54-60.
20 Y. Yuan, H. B. Sun, S. C. Ge, M. J. Wang, H. X. Zhao, L. Wang, L. N. An, J. Zhang, H. F. Zhang, B. Hu, J. F. Wang and G. L. Liang, *ACS Nano*, 2015, **9**, 761-768.
21 Y. L. Xu, H. J. Xu, X. S. Jiang and J. Yin, *Adv. Funct. Mater.*, 2014, **24**, 1679-1686.
22 D. D. Díaz, E. Morin, E. M. Schön, G. Budin, A. Wagner and J.-S. Remy, *J. Mater. Chem.*, 2011, **21**, 641-644.
23 J. Boekhoven, J. M. Poolman, C. Maity, F. Li, L. van der Mee, C. B. Minkenberg, E. Mendes, J. H. van Esch and R. Eelkema, *Nat. Chem.*, 2013, **5**, 433-437.
24 S. Liu, A. M. Tang, M. L. Xie, Y. D. Zhao, J. Jiang and G. L. Liang, *Angew. Chem. Int. Ed.*, 2015, **54**, 3639-3642.
25 M. Reches and E. Gazit, *Science*, 2003, **300**, 625-627.
26 D. Yuan, J. F. Shi, X. W. Du, N. Zhou and B. Xu, *J. Am. Chem. Soc.*, 2015, **137**, 10092-10095.
27 H. J. Liu, Y. H. Hu, H. M. Wang, J. Y. Wang, D. L. Kong, L. Wang, L. Y. Chen and Z. M. Yang, *Soft Matter*, 2011, **7**, 5430-5436.
28 Y. H. Hu, H. M. Wang, J. Y. Wang, S. B. Wang, W. Liao, Y. G. Yang, Y. J. Zhang, D. L. Kong and Z. M. Yang, *Org. Biomol. Chem.*, 2010, **8**, 3267-3271.
29 Z. D. Wu, M. Tan, X. M. Chen, Z. M. Yang and L. Wang, *Nanoscale*, 2012, **4**, 3644-3646.
30 T. Yoshii, M. Ikeda and I. Hamachi, *Angew. Chem. Int. Ed.*, 2014, **53**, 7264-7267.
31 Y. Q. Sun, J. Liu, H. X. Zhang, Y. Y. Huo, X. Lv, Y. W. Shi and W. Guo, *J. Am. Chem. Soc.*, 2014, **136**, 12520-12523.